Li *et al.*
Chinese Journal of Mechanical Engineering (2023) 36:92
https://doi.org/10.1186/s10033-023-00930-5

Chinese Journal of Mechanical Engineering

ORIGINAL ARTICLE

Open Access

Cutting Force Fluctuation Suppression and Error Homogenization of Noncircular Gear Hobbing Based on the Tool Shifting Method

Dazhu Li[1,2], Jiang Han[2*], Xiaoqing Tian[2] and Lian Xia[2]

Abstract

The current research on noncircular hobbing mainly focuses on the linkage model and motion realization. However, the intermittent cutting characteristics of hobbing would increase uncertainties in the manufacturing process. In this paper, a hobbing machining model with tool-shifting characteristics was proposed to solve the problems of cutting force fluctuation and inconsistency of tooth profile envelope accuracy at different positions of the pitch curve in noncircular gear hobbing. Based on the unit cutting force coefficient method, the undeformed chip volume generated by interrupted cutting was used to characterize the fluctuation trend of the hobbing force. The fluctuation characteristics of the cutting force generated by different hobbing models were compared and analyzed. Using the equivalent gear tooth and hob slotting numbers, an analysis model of the tooth profile envelope error of the noncircular gear was constructed. Subsequently, the tooth profile envelope errors at different positions of the pitch curve were compared and analyzed based on the constructed model. The transmission structure of the electronic gearbox was constructed based on the proposed hobbing model, and the hobbing experiment was conducted based on the self-developed noncircular gear CNC hobbing system. This paper proposes a hobbing method that can effectively suppress the fluctuation of the peak and whole circumference cutting force and reduce the maximum envelope error of the whole circumference gear teeth.

Keywords Noncircular gear, Gear hobbing, Cutting force, Envelope error, Machining model

1 Introduction

Noncircular gears have many advantages in solving variable speed ratio transmissions, such as compact structure, good rigidity, high-speed operation, and long life. Their applications include agricultural machinery, automation equipment, robots, and transmissions [1–4]. Presently, the manufacturing of noncircular gears is still mainly based on the forming method, which is based on tooth profile vector graphics. Research on the tooth profile solution of noncircular gears has received extensive attention [5–8], but the tooth-making method, based on the principle of generating machining, has not been widely used. Due to the variety of noncircular shapes and the complexity of tooth profiles, high efficiency, high precision, high flexibility, and mass manufacturing are still barriers to developing noncircular gears.

Generating machining is an efficient gear manufacturing method, which realizes the manufacture of noncircular gears with different pitch curves through the linkage relationship of variable speed ratios between multiple axes[9, 10]. Litvin et al. studied the generating motion process of the rack cutter and the noncircular gear and demonstrated the achievability of noncircular gear hobbing [11]. Tan et al. deduced the simplest mathematical model for noncircular gear hobbing,

*Correspondence:
Jiang Han
jianghan@hfut.edu.cn
[1] Institute of Artificial Intelligence, Anhui Polytechnic University, Wuhu 241000, China
[2] CIMS Institute, Hefei University of Technology, Hefei 230009, China

created the hobbing process using a three-axis linkage method, and conducted a graphic simulation [12]. Hu et al. studied the realization scheme of noncircular gear generation and machining linkage control from the perspective of an electronic gearbox. Furthermore, they provided a diagram of the general principle of computer number control (CNC) linkage control for noncircular helical gear hobbing machining [13]. Han et al. conducted the realization and experimental research of noncircular gear generation processing and used a flexible electronic gearbox to precisely control the transmission ratio linkage [14, 15]. These studies solve the basic problems of noncircular gear hobbing: processing feasibility, hobbing motion, and motion realization process. Presently, scholars' research on noncircular gear hobbing focuses on constructing the hobbing linkage model, the hobbing simulation test, and realizing hobbing motion.

However, due to the intermittent cutting characteristics of hobbing, the cutting force fluctuates greatly during the manufacturing process. Noncircular gear hobbing faces not only the problem of intermittent cutting but also differences in pitch curve positions, making it more complicated than cylindrical gear hobbing. The fluctuating characteristics of the cutting force during noncircular gear hobbing are highly significant. However, the current research on predicting and improving the hobbing force and process of noncircular gears is still lacking.

In addition, intermittent cutting causes the tooth profile of noncircular gears to be composed of tiny line segments formed by multiple cuts, and the theoretical tooth profile is the envelope curve of these polylines, which causes machining principle error in the hobbing process [16]. This error can also be called envelope error. For noncircular pitch gears, the motion of the hob relative to the noncircular pitch gear has nonlinear characteristics due to the difference in the pole diameter and curvature radius at different positions of the pitch curve. This will cause the hob to have different cutting characteristics for the tooth profiles at different positions of the pitch curve, resulting in unequal envelope errors.

In this paper, a noncircular gear hobbing model with the tool shifting method is proposed, which can realize the constant arc length processed by the hob on the noncircular pitch curve per unit time. The realization of this characteristic can make the hob have similar cutting conditions at different pole diameter length positions of the noncircular gear and produce relatively similar cutting times on the tooth surfaces at different positions. Therefore, the problems of large fluctuation of cutting force and uneven distribution of envelope errors in noncircular gear hobbing are improved.

2 Derivation of the Constant Arc Length Incremental Hobbing Model

Noncircular gear hobbing can be regarded as the meshing transmission process between the worm and the noncircular gear, in which the worm rotates to form the cutting motion and moves in the direction of the gear axis to form the machining of the full tooth width. Considering the movement of each cutting linkage axis, the biggest difference between the noncircular gear and the cylindrical gear is that the tool has a linkage movement relative to the gear blank in X-axis direction (Figure 1).

Similar to cylindrical gear hobbing, the projection of the hob on the end section of the noncircular gear can still be regarded as an equivalent rack. Therefore, the spatial meshing motion of the worm and noncircular gear is equivalent to the plane meshing motion of the rack and the end-section gear and can be regarded as a pure rolling process between the centerline of the rack and the noncircular pitch curve (Figure 2).

In the coordinate system S-XOY, the center line of the hob-projected rack and the noncircular pitch curve conduct pure rolling from point A of the pitch curve to point B (Figure 2). The polar diameter corresponding to point B is r, the polar angle is ϕ, and the angle between the polar diameter and the tangent is μ. Under the condition of no tool shifting, the noncircular gear hobbing model is calculated as follows [12, 17]:

$$\begin{cases} \omega_{\mathrm{C}} = \dfrac{\sqrt{r^2 + (\mathrm{d}r/\mathrm{d}\varphi)^2}}{r^2}\left(\mathrm{K_C}\omega_{\mathrm{B}}\dfrac{Tm_{\mathrm{n}}}{2\cos\beta} + \mathrm{K_Z}v_{\mathrm{Z}}\tan\beta\right), \\ v_{\mathrm{X}} = \dfrac{\mathrm{d}r/\mathrm{d}\varphi}{r}\left(\omega_{\mathrm{B}}\dfrac{\mathrm{T}m_{\mathrm{n}}}{2\cos\beta} + \mathrm{K_Z}v_{\mathrm{Z}}\tan\beta\right), \end{cases} \tag{1}$$

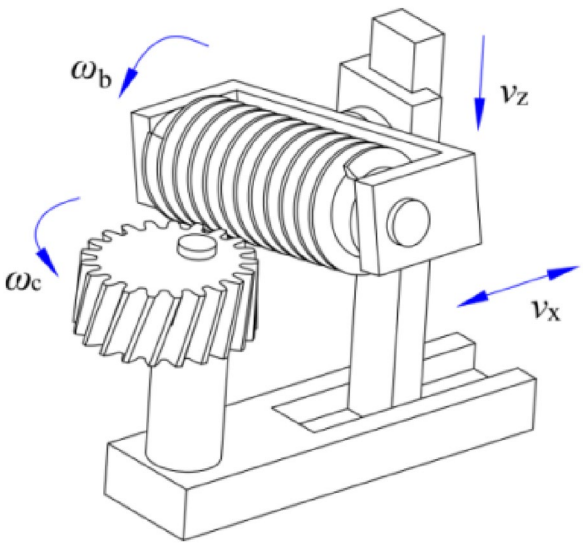

Figure 1 Linkage model for noncircular gear hobbing

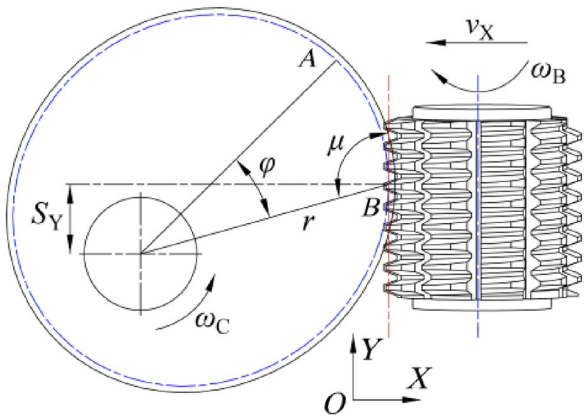

Figure 2 Meshing projection of the tooth blank-end face

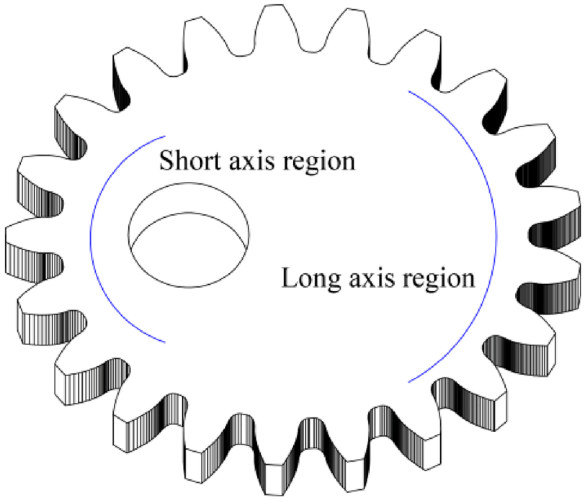

Figure 3 Simulation results of elliptical gear based on Eq. (1)

where, m_n refers to the normal modulus; β refers to the helix angle; T refers to the number of hob heads, and K_Z and K_C are the sign coefficients related to the climb or up milling methods and the helical direction of the hob.

According to Eq. (1), the feed motion of the hob in the direction of the gear axis will simultaneously generate additional motion in the direction of the gear rotation C axis and hob movement X axis. This feature is the main difference from the additional motion form during cylindrical gear hobbing. During the machining process based on the hobbing model described in Eq. (1), the distance S_Y between the tangent point between the center line of the rack and the pitch curve and the X-axis shown in Figure 2 is always changing, which leads to the arc length of the rack center line rolling on the pitch curve in unit time is always varying.

Taking the hobbing of elliptical gears as an example, due to the fluctuation of the arc length increment per unit time, the hobbing process will produce unequal cutting times at the long and short axes of the ellipse pitch curve, which will induce cutting force fluctuation and envelope error. The cutting traces of the elliptical gear tooth surface obtained based on the solid simulation machining method are shown in Figure 3.

The number of cutting times of the hob at the long axis of the elliptical gear is considerably more than that at the short axis (Figure 3). This is due to the combined effect of the characteristics of the noncircular gear pitch curve and the adopted hobbing model. Figure 4 shows the incremental change of the arc length per unit time at different positions of the pitch curve during the cycle machining process of the elliptical gear.

As shown in Figure 4, the arc length increment per unit time at the long axis is smaller than that at the short axis. Furthermore, the smaller the arc length increment, the denser the cutting marks. When the unit time is defined as the time difference between the two adjacent rows of cutting edges in the circumferential direction of the hob passing the same position, the value of the arc length increment will be closely related to the density of the tooth surface cutting marks. If a consistent arc length increment per unit time is obtained at different positions of the noncircular pitch curve, it can benefit the homogenization of the cutting force and the envelope error of the noncircular gear.

During noncircular gear hobbing, the hob rotates at a constant speed. The realization of the constant arc length increment ensures that the displacement generated by the hob projection rack in Y-axis per unit time equals the arc length increment of the noncircular pitch curve. That is, the tangent point of the cylindrical surface corresponding to the pitch circle of the hob and the noncylindrical surface corresponding to the noncircular pitch curve need to remain unchanged relative to the hob, the same with the cylindrical gear hobbing process. Compared with the introduction of the hobbing model

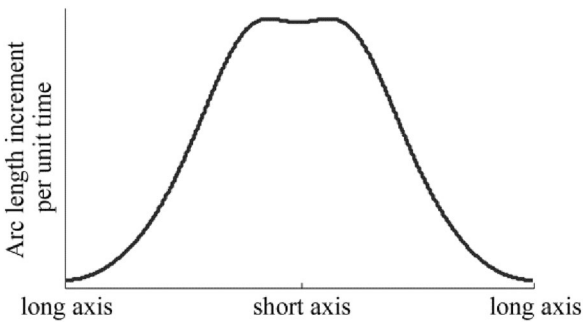

Figure 4 Incremental change of the arc length in elliptical gear hobbing based on Eq. (1)

in Figure 2, it can be seen that to achieve a constant arc length increment, the cutter axis needs to participate in the linkage. On the premise that the machine tool has sufficient tool-shifting ability, the tangent point between the center line of the rack and the noncircular pitch curve is always kept at the same point on the rack during the hobbing process. That is, at different positions of hob processing, the hob shaft will have a time-varying tool-shifting motion (Figure 5).

Given a constant arc length increment, hobbing starts from point A on the pitch curve, and point B is any point on the pitch curve (Figure 5). If a vertical line is drawn through point A that is perpendicular to the pitch line of the projected rack, the distances from the vertical line to the left and right sides of the hob are S_{AL} and S_{AR}, respectively. The S_{BL} and S_{BR} corresponding to point B are obtained similarly, and there are numerical relationships S_{AL}=S_{BL} and S_{AR}=S_{BR}. The realization of this equal relationship can be solved by compensating for the distance S_{Y} described in Figure 2 through the hob shifting movement. The calculation formula of S_{Y} is as follows:

$$S_{\mathrm{Y}} = r\cos\mu = r\frac{\mathrm{d}r}{\mathrm{d}\varphi}/\sqrt{r^2+(\mathrm{d}r/\mathrm{d}\varphi)^2}. \tag{2}$$

Eq. (2) is derived from ϕ to obtain the following:

$$v_{\mathrm{Y}}(\varphi) = \frac{(\frac{\mathrm{d}r}{\mathrm{d}\varphi})^2}{(r^2+(\frac{\mathrm{d}r}{\mathrm{d}\varphi})^2)^{\frac{1}{2}}} + \frac{r\frac{\mathrm{d}^2r}{\mathrm{d}\varphi^2}(r^2+(\frac{\mathrm{d}r}{\mathrm{d}\varphi})^2) - r(\frac{\mathrm{d}r}{\mathrm{d}\varphi})^2 - (\frac{\mathrm{d}r}{\mathrm{d}\varphi})^2\frac{\mathrm{d}^2r}{\mathrm{d}\varphi^2}}{(r^2+(\frac{\mathrm{d}r}{\mathrm{d}\varphi})^2)^{\frac{5}{2}}}. \tag{3}$$

Eq. (3) can be understood as the additional moving speed of the projection rack in Y-axis by the hob shifting motion. Substitute Eq. (3) into Eq. (1) to obtain the linkage model of hob shifting compensation:

$$\begin{cases} \omega_{\mathrm{C}} = \dfrac{\sqrt{r^2+(dr/d\varphi)^2}}{r^2} \times (\mathrm{K_C}\omega_{\mathrm{B}}\dfrac{Tm_{\mathrm{n}}}{2\cos\beta} + \mathrm{K_Y}v_{\mathrm{Z}}\tan\beta + v_{\mathrm{Y_B}}\dfrac{\cos\lambda}{\cos\beta}), \\ v_{\mathrm{X}} = \dfrac{\mathrm{d}r/\mathrm{d}\varphi}{r}(\omega_{\mathrm{B}}\dfrac{Tm_{\mathrm{n}}}{2\cos\beta} + \mathrm{K_Y}v_{\mathrm{Z}}\tan\beta + v_{\mathrm{Y_B}}\dfrac{\cos\lambda}{\cos\beta}), \\ v_{\mathrm{Y_B}} = v_{\mathrm{Y}}(\varphi)\dfrac{\cos\beta}{\cos\lambda}, \end{cases} \tag{4}$$

where λ refers to the installation angle of the hob.

3 Modeling of the Hobbing Process and Evaluation of Cutting Force Fluctuations

3.1 Geometric Information Acquisition of Undeformed Chips

The unit cutting force coefficient method is common for solving the cutting force in the metal cutting process. The method converts the calculation of cutting force into the superposition of cutting force per unit area. Additionally, it solves the overall cutting force by solving the cutting force vector sum of each micro-element cutting edge. The cutting process of the hob cutting edge belongs to the inclined edge non-free cutting. The right-angle orthogonal cutting theoretical model commonly used in the research of metal cutting mechanisms is no longer applicable, and the current mathematical model widely used to analyze the cutting force of gear hobbing is the Kienzle–Victor cutting force empirical formula [18]. This formula establishes the link between the cutting force and the geometry of the undeformed chip produced by the cutting process.

The hobbing process is intermittent cutting, which has a certain similarity with the milling process. The development of its cutting simulation needs to be based on the solid model of the gear blank and the cutting path model of the hob. According to the hob design and process parameters, the cutting trajectory of a row of cutting edges can be constructed. When the hob rotates through a row of teeth, the cutting trajectory of the next row of teeth can be regarded as the movement of the cutting trajectory corresponding to the previous row of teeth in the direction of the hob axis. Assuming that the hob used in the simulation is a straight groove zero rake angle hob, the axial truncation of the hob in the chip flute can be regarded as a standard rack. Considering the rotation of the hob and the axial feed motion of the rack, the spatial trajectory of a point on the rack can be obtained. Then, a solid model of the cutting trajectory can be obtained by scanning the rack along the trajectory.

The solid models of the gear blank and cutting path are assembled to form a solid model for hobbing cutting simulation. Cutting the tooth blank by the hob is divided into the cut-in stroke, the complete cut-in stroke, and the cut-out stroke according to the different feed positions in Z-axis direction. The solid model in the full cut-in stroke is shown in Figure 6.

As shown in Figure 6, in the Cartesian coordinate system constructed with the rotation center of the gear blank as the coordinate origin, when the hob completes an intermittent cutting, the required stepping motion is as follows: (1) The step rotation of the gear blank in C axis direction; (2) The step movement of the cutting trajectory solid in the hob axis Y_{B} axis

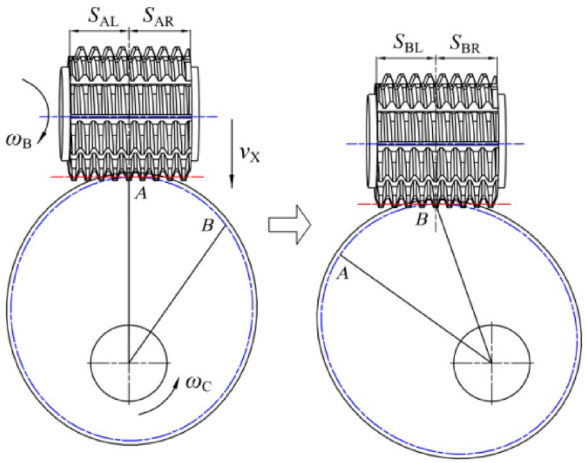

Figure 5 Hob position feature with constant arc length increment

direction; (3) The step movement of the cutting trajectory solid in Z axis direction; (4) The step movement of the cutting trajectory entity in X-axis direction. Taking the hob rotating through a single row of teeth as the step unit, the gear blank and the cutting trajectory solid are moved step by step, and after each step movement is completed a solid subtraction operation is performed to realize one cutting.

The above process simulates the cutting characteristics of the hob in the full plunge state. At the beginning of the simulation, the gear blank is in a total state; however, in the actual hobbing process, the hob adopts a step-by-step cut-in method in Z-axis direction. In order to obtain the chip model generated by the interrupted cutting when the hob is fully plunged, the two-cycle hobbing simulation method was adopted. That is, based on the hobbing simulation of the first circle, the gear blank model obtained by the first circle simulation is used as a new gear blank, and the second

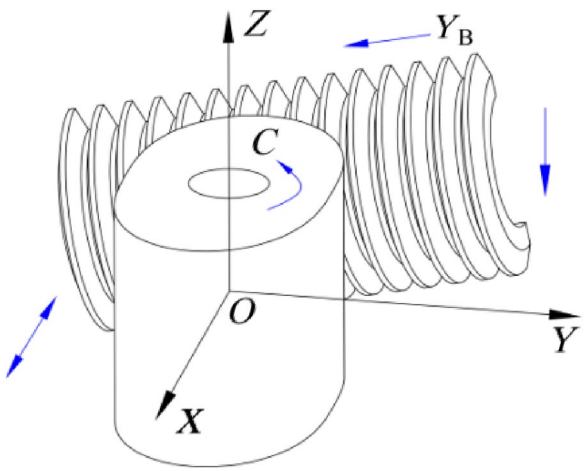

Figure 6 Model for the simulation of noncircular gear hobbing

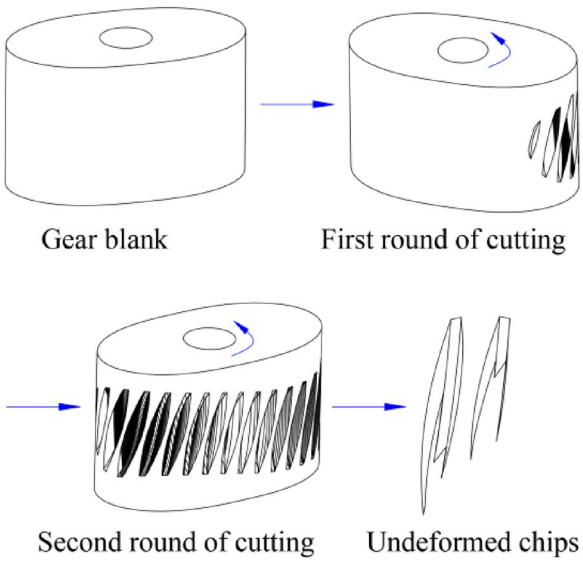

Figure 7 Extraction process of undeformed chip geometry

circle simulation is conducted. During the second circle simulation, the overlapping part of the two solids can be obtained through the intersection operation, which is the undeformed chip corresponding to this cutting step. The process is illustrated in Figure 7.

3.2 Evaluation of the Fluctuating Characteristics of the Cutting Force

During the hobbing simulation, the undeformed chip volume produced by an interrupted cut is the available data. In this paper, the positive correlation between the undeformed chip volume and the cutting force value is a sufficient condition for analysis. This is because when the hob is in the full cut-in state, the length of the chips generated by each tooth of the integral hob in the direction of the gear axis is the same or a small multiple. The factors affecting the undeformed chip volume of a certain cutting behavior can be summarized into (a) the increase of the average area of each section layer of the chips generated by each cutter tooth and (b) the increase of the number of cutter teeth involved in cutting. Between them, condition (b) is acting on condition (a), and if condition (a) is established, it is acting on the probability of the maximum cutting area of a certain section. The empirical formula of the Kienzle–Victor cutting force is as follows [19]:

$$\begin{cases} Fc = A \times Ks, \\ Ks = Kc/h^u, \end{cases} \tag{5}$$

where, Fc is the main cutting force (N); A is the cutting area(mm^2); Ks is the specific cutting force (N/mm^2), and

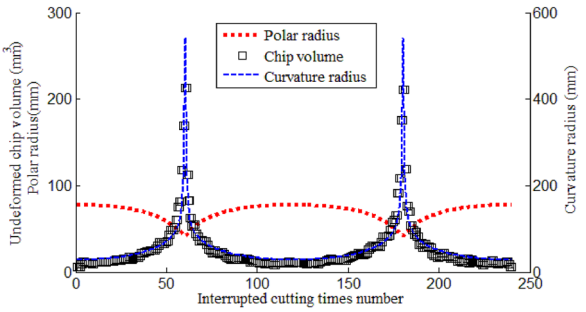

Figure 8 Variation of the chip volume corresponding to Eq. (1)

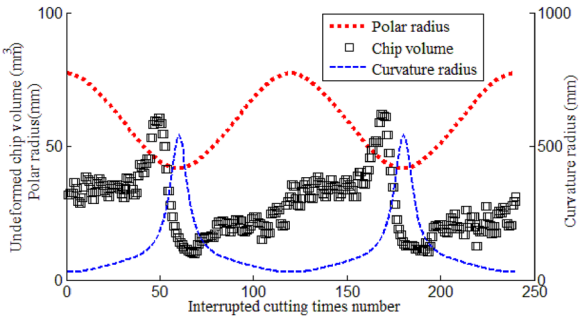

Figure 9 Variation of the chip volume corresponding to Eq. (4)

*K*c is the cutting force corresponding to a unit section. The nominal thickness and width of the unit section are both 1 mm, *h* is the cutting layer thickness (mm), and *u* is the fixed value coefficient, reflecting the influence of *h* on *K*s. The values of *K*c and *u* are determined by the workpiece material and can be obtained using the experimental method.

According to Eq. (5), the cutting area corresponding to a certain section has a dominant influence on the current cutting force, and the influence of the cutting layer thickness is insignificant. For example, the constant value coefficient *u* in Eq. (5) is taken as 0.2. When the thickness of the cutting layer changes from 0.02 mm to 0.2 mm, the influence on the cutting force calculation is only 1.58 times. In the following, the whole cycle cutting simulation of the oval gear is conducted, and the variation law of the chip volume during the simulation process is analyzed. The important design parameters of oval gear and hob are shown in Table 1.

Provided that the hob fully cuts into the oval gear, the cutting trajectory solid model and the gear blank are constrained by Eqs. (1) and (4) to conduct a two-cycle cutting simulation, respectively. Record the volume changes of the gear blank generated by each step in the second circle simulation, and display the change of the chip volume, the curvature radius, and the polar radius corresponding to each interrupted cutting position on the same graph.

Table 1 Design parameters of the simulation model

Noncircular gear		**Hob**	
Number of teeth	30	Thread number	1
Normal modulus (mm)	4	Slots number	8
Helical angle	15°	Thread pitch (mm)	12.5788
Pitch curve	Oval ellipse	Helical angle(°)	2.5473
Eccentricity	0.3	Outer diameter(mm)	100
Helical direction	Right	Helical direction	Right

The simulation results of Eqs. (1) and (4) are shown in Figures 8 and 9, respectively.

The analysis in Figure 8 shows that the chip volume generated by each interrupted cutting is consistent with the changing trend of the curvature radius of each position. The undeformed chip volume produced by each interrupted cut is proportional to the curvature radius of the pitch curve at that position and inversely proportional to the polar radius. The peak cutting force occurs at the shortest axis during the cutting cycle.

The analysis in Figure 9 shows that for the constant arc length increment model, the maximum position of the curvature radius is not the maximum position of the chip volume, and the positive correlation between the chip volume and the curvature radius is not maintained. The maximum and minimum positions of the chip volume are located at approximately symmetrical positions on both sides of the maximum curvature radius. In addition, the positions of the maximum cutting volume and minimum chip volume are located on the cut-in and cut-out sides of the hob, respectively. The unevenness of the chip volume at different positions of the pitch curve is greatly improved, the ratio of the maximum to the minimum chip volume is reduced from 19.3 to 6.2 times, and the stability of the noncircular gear hobbing process can be improved.

4 Theoretical Envelope Error Modeling and Comparative Analysis

4.1 Geometric Simulation of the Envelope Generated by Hob Cutting

The shape of the hob can be regarded as the circumferential arrangement of the single row of cutter teeth in the direction of the hob axis along the direction of the helical line. Interrupted cutting is the root cause of the theoretical error of tooth profile machining. In order to realize the equivalent simulation of interrupted cutting, the cutting behavior of the hob is equivalent to that of the rack

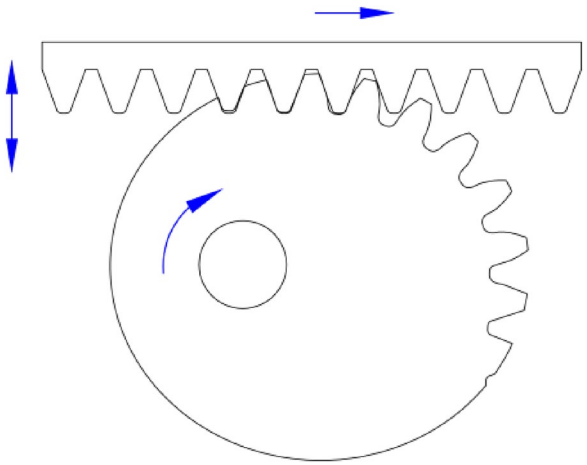

Figure 10 Visualized tooth profile shaping of the equivalent rack cutter

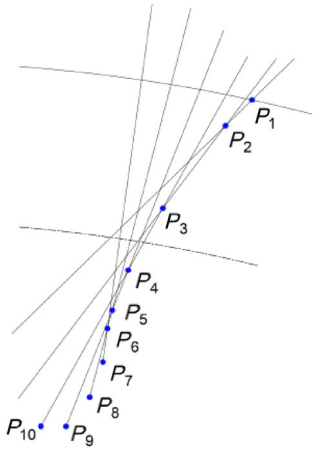

Figure 12 Definition of feature points on the tooth profile

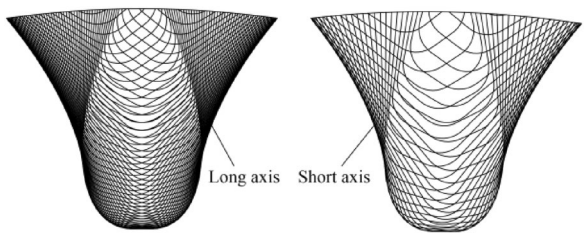

Figure 11 Envelope trajectory of the rack cutter at the long and short axis positions

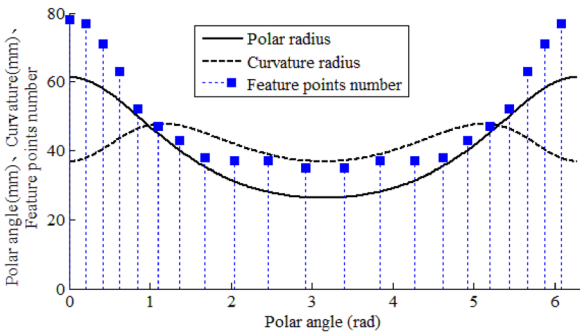

Figure 13 Number distribution of feature points on the tooth profile

cutter in this paper. The hob flute divides the hob into K rows of cutting teeth. Assuming that the current first row of teeth is in the cutting state, when the hob rotates through an angle of 2π/K, the second row of teeth will be in the position of the current first row of teeth. For the rack cutter equivalent to the first and second rows of teeth of the hob, the translation displacement of the rack cutter can be regarded as π*m*/K.

Based on the constructed digital model of the tool and gear blank, the visual enveloping machining of the tooth profile can be carried out using the Boolean geometric operations [20]. Taking the straight tooth elliptical gear as an example for simulation, the parameters of the elliptical gear are as follows: the teeth number is 21, the modulus is 4 mm, and the eccentricity is 0.4. The main parameters of the hob are as follows: the heads number is 1, and the circumferential slots number is 12. According to the model shown in Eq. (1), the visual envelope processing of the elliptical gear end face tooth profile is carried out. The forming process is as follows.

In the visual forming process of the tooth profile, the Boolean geometry operation between the rack cutter and the gear blank can be canceled, and the enveloping trajectory of the rack cutter on the entire pitch curve can be obtained. The tooth profile envelope trajectory of the elliptical gear at the long and short axes generated by the envelope process shown in Figure 10 is shown in Figure 11.

In order to quantitatively analyze the envelope distribution of each tooth profile, the concept of forming feature points on the tooth profile is introduced. The partially enlarged schematic diagram of the envelope process is shown in Figure 12.

As shown in Figure 12, the intersection point of the rack profile and the gear's outer contour is point *P*1, and the tooth profile intersection *P*2–*P*6 of the two adjacent cutting positions of the slotting cutter tooth profile forms the meshing part tooth profile. The intersection points *P*7–*P*10 of the two adjacent cutting positions of the tooth tip fillet of the slotting cutter form the tooth root. These three types of points are collectively referred to as the hobbed tooth profile forming feature points

of noncircular gears. Based on the tooth profile vector graphics generated by the simulation, the number N of the tooth profile forming feature points of each tooth slot is statistically extracted. In order to analyze the comprehensive relationship between the number of feature points at different positions of the pitch curve and the polar and curvature radii, the changing trends of these three are expressed in a graph, with the polar angle as the independent variable (Figure 13).

An analysis of Figure 13 shows that the density of the tooth surface envelope is positively correlated with the polar radius of the pitch curve. The envelope is dense at the position with a large polar radius and sparse at the position with a small polar radius. The ratio of the number of feature points is approximately equal to the ratio of the length of the polar radius. The curvature radius at different positions of the pitch curve has no obvious relationship to the density distribution of the envelope. For example, the elliptical gear has the same curvature radius at polar angles of 0° and 180°, but the envelope distribution of the tooth surface is quite different.

4.2 Mathematical Modeling and Fluctuation Analysis of Tooth Envelope Error

The tooth profiles of noncircular gears are different, and selecting a suitable analysis object when evaluating the approximation error from the feature point to the theoretical tooth profile is difficult. The modulus of each tooth of a noncircular gear is the same. However, it has the particularity of variable curvature and polar radii, which leads to the distribution of its envelope error related to its design parameters and the hobbing linkage model. For example, for the elliptical gear process based on Eq. (1) and shown in Figure 11, although the curvature radius and the theoretical tooth shape are the same at the long and short axes, there is a big difference in the density of the tooth surface envelope. In this paper, the concept of equivalent gear is used to analyze the tooth profile envelope error of noncircular gears.

Here, based on the equivalent circular gear with the teeth number z_d defined by the curvature radius, the equivalent hob slot number K_d, which is jointly defined by the pitch curve parameters and the hobbing linkage model, is proposed. This method can comprehensively consider the common influencing factors of the hobbing linkage model, the polar and curvature radii of the pitch curve, and the parameters of the hob. The parameter definition analysis is shown in Figure 14.

Figure 14 shows that when the hob rotates through a row of teeth, the arc length change of the noncircular pitch curve is ΔS, and the calculation of z_d and K_d is as follows:

$$\begin{cases} z_d = 2\rho/m, \\ K_d = \pi m/\Delta S, \\ \Delta S = \pi m/K + r_1 \cos\mu_1 - r\cos\mu, \end{cases} \tag{6}$$

where, the polar radius corresponding to the position of the polar angle ϕ is r, the curvature radius is ρ, and the angle between the polar radius and the tangent is μ. The polar radius corresponding to the position of the polar angle ϕ_1 is r_1, and the angle between the polar radius and the tangent is μ_1.

Taking the simulated elliptical gear shown in Figure 10 as an example, the calculation results of the equivalent gear tooth and hob slot numbers at each position during the hobbing process based on Eq. (1) are shown in Figure 15.

Figure 15 shows that, for an elliptical gear, when the positions of the long and short axes are the same as the number of teeth of the equivalent gear, the equivalent number of tooth slots of the hob is about 2.5 times

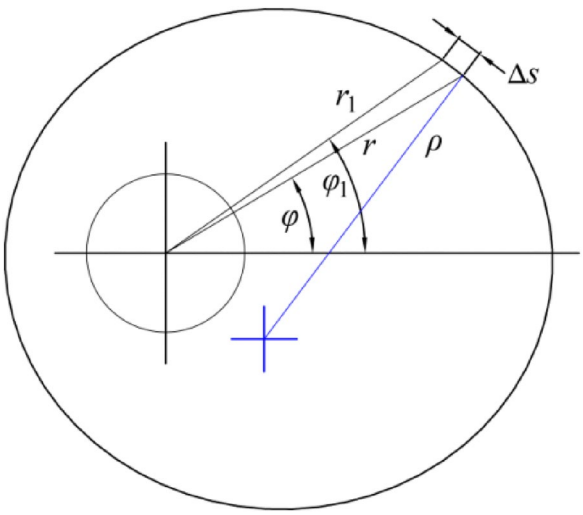

Figure 14 Equivalent parameter calculation diagram

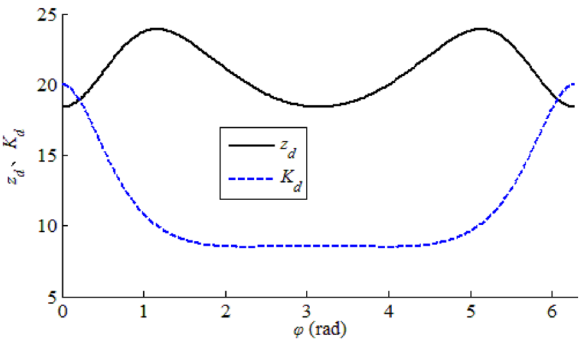

Figure 15 Calculation examples of z_d and K_d

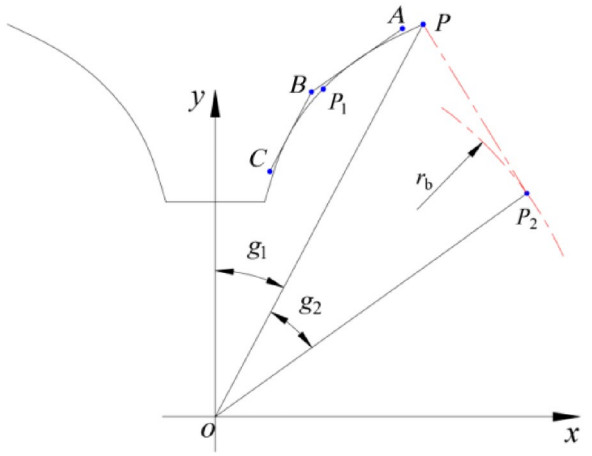

Figure 16 Polyline envelope forming the theoretical tooth profile

different. This equates to approximately 2.5 times the number of cuts per tooth profile at the long axis than at the short axis. Simultaneously, the proportional relationship is consistent with the proportional relationship of the number of tooth surface feature points obtained by the hobbing simulation shown in Figure 13, which can illustrate the rationality of the equivalent hob slot number mentioned in the paper.

The theoretical tooth profile of a noncircular gear is a tangent curve of a polyline formed by connecting the feature points of each tooth profile end-to-end. The relationship between the polyline and the theoretical tooth profile is shown in Figure 16.

Figure 16 shows that the theoretical tooth profile is tangent to the line segments *AB* and *BC*, the polyline *ABC* is the actual tooth profile generated by hobbing, and the tooth profile envelope error is defined as the closest distance from the feature point to the theoretical tooth profile. In the coordinate system, *s-xoy*, the tooth profile of a tooth slot is symmetrically distributed relative to the *y*-axis, the point *P* is the vertex of the tooth profile, the point P_1 is any point on the theoretical tooth profile, and the point P_2 is the tangent point between the tooth profile normally passing through the point *P* and the base circle. The included angle between line *oP* and *y*-axis is g_1, and the included angle between line *oP* and oP_2 is g_2, i.e., the pressure angle corresponding to point *P*. The coordinates (x_1, y_1) of the point P_1 can be expressed as a function of the pressure angle α_1 about this point [20]:

$$\begin{cases} x_1 = r_b/\cos\alpha_1 \sin(\text{inv}\alpha_1 + \Delta\theta), \\ y_1 = r_b/\cos\alpha_1 \cos(\text{inv}\alpha_1 + \Delta\theta), \\ \alpha_1 \in [0, g_2], \\ \Delta\theta = g_1 - \text{inv}g_2. \end{cases} \tag{7}$$

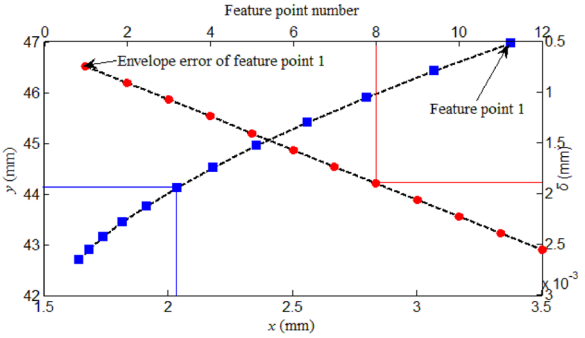

Figure 17 Tooth profile feature points and errors of the calculation example

Let the coordinates of point *B* be (x_0, y_0), then the distance from this point to each point on the theoretical tooth profile can be expressed as a function of α_1:

$$f(\alpha_1) = \sqrt{(x_0 - x_1)^2 + (y_0 - y_1)^2}, \tag{8}$$

where, the minimum value of this function is called the envelope error δ from the tooth profile feature point to the theoretical tooth profile. Let $f'(\alpha_1)=0$, then the pressure angle α_1 of the closest point from the characteristic point on the theoretical tooth profile can be obtained, and the approximation error can be solved by Eqs. (7) and (8).

To conduct a calculation following the above method, take z_d=30 and K_d=7 and define the modulus as 4 mm, the pitch circle pressure angle as π/9, and the addendum height coefficient as 1. Twelve tooth profile feature points can be obtained in the meshing part of the unilateral tooth profile. Define the rightmost point of the *x*-axis as Point 1 and the leftmost point as Point 12. The coordinates and errors of these points are shown in Figure 17.

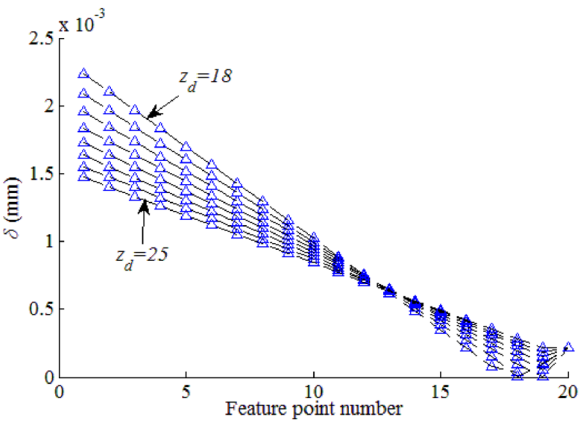

Figure 18 The effect of z_d change on δ

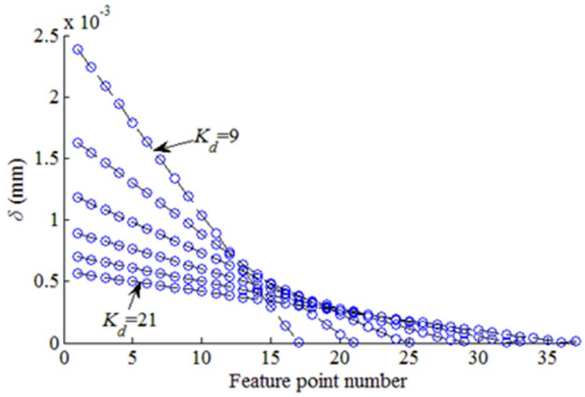

Figure 19 The effect of K_d change on δ

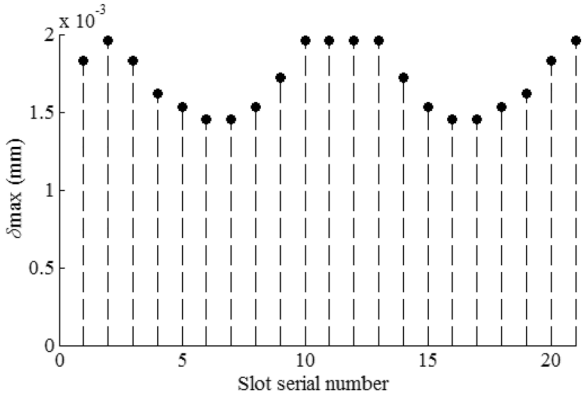

Figure 21 Maximum envelope error of each tooth profile based on Eq. (4)

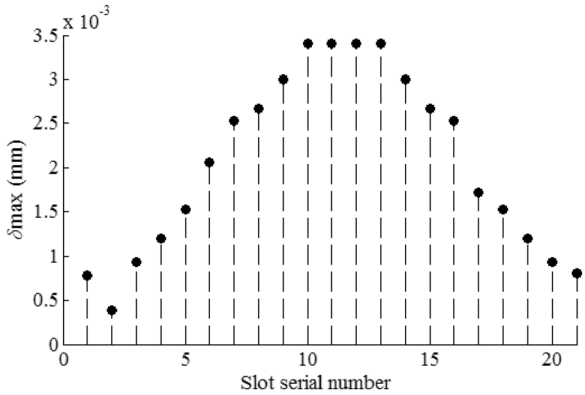

Figure 20 Maximum envelope error of each tooth profile based on Eq. (1)

Figure 22 Hobbing experimental platform of the oval gear

As shown in Figure 17, the envelope error generated by hobbing has a decreasing trend from the tooth tip to the tooth root, and the maximum envelope error $\delta_{\max}$ is 0.00256 mm. The envelope error of the tooth profile at different positions of the noncircular gear is related to the z_d and K_d of the position. In order to determine the position and value of the $\delta_{\max}$ of the noncircular gear, the influence of z_d and K_d on the $\delta_{\max}$ is analyzed following the control variable method. Based on the parameters used in the calculation in Figure 17, let K_d=10, z_d=18~25, and take the step size as 1; the error of each feature point is as shown in Figure 18.

Let z_d=20, K_d=9~21, and take the step size as 2; the error of each feature point is as shown in Figure 19.

Through the analysis of Figures 18 and 19, the following can be summarized. (1) When K_d is constant, the change of z_d has almost no effect on the number of tooth profile feature points generated by the envelope; however, $\delta_{\max}$ decreases with the increase of z_d. (2) Provided that z_d remains unchanged, the increase of K_d will increase the number of tooth profile feature points, and $\delta_{\max}$ will decrease with the increase of K_d.

Following this conclusion, for the elliptical gear, the maximum value of the tooth profile envelope error will appear near the short axis because z_d and K_d are the smallest at this position. According to the data shown in Figure 15, take z_d=19, K_d=9, and $\delta_{\max}$=0.00342 mm. The tooth slot at the long axis of the elliptical gear is taken as the first tooth slot, and the numbers increase in the counterclockwise direction. The maximum envelope error of each tooth profile is shown in Figure 20.

As shown in Figure 20, for the elliptical gear analysis example selected in this paper, $\delta_{\max}$ shows an increasing trend from the long axis to the short axis in the case of double fluctuations of z_d and K_d.

Taking the case of the selected elliptical gear, the calculation of the envelope error is conducted based on the constant arc length incremental hobbing model shown in Eq. (4). At this time, the K_d value of the entire circumference of the elliptical gear is 12. According to the change rule that $\delta_{\max}$ decreases with the increase of z_d, it can be known that $\delta_{\max}$ will appear at the position where z_d is smallest; thus, the maximum envelope error of each tooth profile is shown in Figure 21.

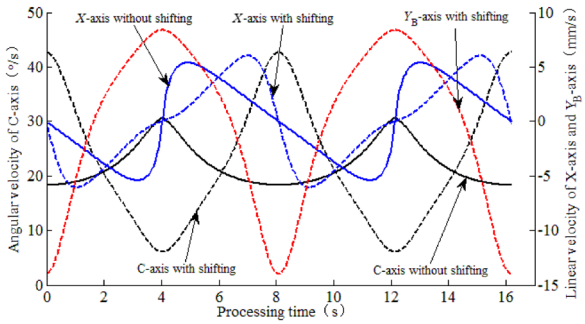

Figure 23 Speed variation characteristics of each axis under the two hobbing models

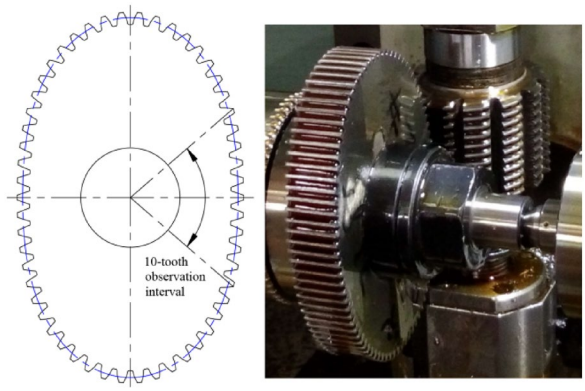

Figure 24 Oval gear hobbing near the shortest axis

As shown in Figure 21, in the simulation calculation of the envelope error based on the model shown in Eq. (4), the δ_{max} of the entire circumference tooth profile is 0.0019 mm, which is 0.00152 mm lower than that before the improvement. The maximum envelope error is located at the long and short axes of the elliptical gear.

5 Experimental Analysis

In order to verify the relevant conclusions about the cutting force and envelope error in the hobbing of noncircular gears analyzed above, this section takes oval gears as the experimental research object on hobbing. Based on Eqs. (1) and (4), the control model of the electronic gearbox was built, and processing experiments were conducted. The experimental platform is based on the YN3610 CNC gear hobbing machine of Nanjing No. 2 Machine Tool Co., Ltd. and equipped with the gear machining CNC system independently developed by the CIMS Research Institute, Hefei University of Technology [14]. The experimental platform and process are shown in Figure 22.

The main design parameters of the hobbed oval gear are as follows: the number of teeth is 54, the modulus is 1 mm, the eccentricity is 0.25, the long axis is 32.7708 mm, and the short axis is 19.6625 mm. Setting the rotating speed of the hob used was 200 r/min, and the cutting depth was 0.5 mm, the speed variation characteristics of each axis corresponding to the two hobbing models are as follows (Figure 23).

By comparing the speed curves of each axis under the two hobbing models as follows: for the *C*-axis, the two models have opposite trends of speed change, and the tool shifting method changes the speed change trend under the condition of no shifting method; for the *X*-axis, the trend of speed change of the two models is similar, but the tool shifting method changes the position of the high and low points of the speed under the condition of no tool shifting. In the processing experiment based on the hobbing model described in Eq. (1), when the processing was near the shortest axis, the machine tool produced a lot of abnormal noise and vibration. According to the analysis of Figure 8, it can be seen that the sudden and large increase of the cutting force near the shortest axis position is the cause of this phenomenon. The hobbing condition of the short axis position is shown in Figure 24.

In the machining experiments based on the model described in Eq. (4), under the same rotational speed and cutting depth of the hob, the abnormal noise and large vibration that occurred when the hob passed near the short axis were not present. The time for the hob to pass through the 10 tooth slots near the short axis shown in Figure 24 is extended from about 1 s to about 3 s. Under the constant rotation speed of the hob, the prolongation of the local hobbing time can indicate that the chip volume generated by each interrupted cut in the hob cutting process has been greatly reduced, thereby improving the cutting stability and suppressing the peak cutting force.

In addition, through an extension of the time in the area near the short axis and the shortening of the time in the area near the long axis, it can be reflected from the side that the intermittent cutting process of the hob can form a denser envelope on the tooth profile surface near the short axis. The envelope density of the tooth profile near the long axis is thinned, which has a homogenizing effect on the entire circumference of the tooth profile envelope error and suppresses the maximum envelope error. The tooth surface roughness of the processed oval

gears at different positions on the entire circumference is relatively consistent and reaches Ra1.6.

6 Conclusions

(1) The time-varying tool-shifting method is adopted to improve the inconsistency of the arc length increment of the pitch curve per unit time caused by the noncircular shape feature. Thus, an incremental hobbing machining model with constant arc length per unit time is proposed.

(2) Based on the unit cutting force coefficient method, a fluctuation analysis of noncircular gear hobbing force is conducted, and a simulation strategy is proposed to obtain the geometric parameters of undeformed chips during noncircular gear hobbing. A comparative analysis of the cutting force fluctuations of the hobbing model before and after optimization is conducted. The constant arc length incremental hobbing model has a significant suppression effect on the cutting force fluctuation, especially the step fluctuation of the cutting force near the large radius of curvature.

(3) Based on the equivalent gear teeth and hob slot numbers, a mathematical model for analyzing the noncircular gear tooth profile envelope error is constructed, and the equivalent hob slot number is affected by the hobbing model. The control variable method is used to study the influence of different parameters on the envelope error, and the analysis strategy of the maximum envelope error of the noncircular gear is obtained. The constant arc length incremental hobbing model can produce the same number of equivalent hob grooves at different positions of the pitch curve so that the envelope error fluctuation is only affected by the change of the curvature radius at different positions, which has a significant effect on the homogenization of the entire envelope error and the suppression of the maximum envelope error.

Acknowledgements
Thanks to Nanjing No. 2 Machine Tool Co., Ltd. for providing support for the experiments of this paper.

Author Contributions
JH was in charge of the whole trial; DL wrote the manuscript; XT and LX assisted with sampling and laboratory analyses. All authors read and approved the final manuscript.

Authors' Information
Dazhu Li, born in 1990, is currently a lecturer at *Institute of Artificial Intelligence, Anhui Polytechnic University, China*. He received his doctor degree from *Hefei University of Technology, China*, in 2022. His research interests include noncircular gear and intelligent manufacturing.
Jiang Han, born in 1963, is currently a professor at *CIMS Institute, Hefei University of Technology, China*.
Xiaoqing Tian, born in 1987, is currently a associate professor at *CIMS Institute, Hefei University of Technology, China*.
Lian Xia, born in 1964, is currently a professor at *CIMS Institute, Hefei University of Technology, China*.

Funding
Supported by National Natural Science Foundation of China (Grant Nos. 52075142 and U22B2084).

Declarations

Competing Interests
The authors declare no competing financial interests.

Received: 31 July 2022 Revised: 26 July 2023 Accepted: 27 July 2023
Published online: 18 August 2023

References

[1] D Mundo, G Gatti, D B Dooner. Optimized five-bar linkages with noncircular gears for exact path generation. *Mechanism and Machine Theory*, 2009, 44(4): 751-760.
[2] F Y Zheng, L Hua, X H Han. The mathematical model and mechanical properties of variable center distance gears based on screw theory. *Mechanism and Machine Theory*, 2016, 101: 116-139.
[3] H Z Song, J G Zheng, W Shi, et al. Design and research of variable speed device based on spiral noncircular gear. *Journal of Mechanical Engineering*, 2017, 53(23): 101-107.
[4] H Terada, Y Zhu, M Suzuki, et al. Developments of a knee motion assist mechanism for wearable robot with a noncircular gear and grooved cams. *Mechanisms and Machine Science*, 2012, 3: 69-76.
[5] B W Bair. Computerized tooth profile generation of elliptical gears manufactured by shaper cutters. *Journal of Materials Processing Technology*, 2002, 122(2-3): 139-147.
[6] B W Bair, C F Chen, S F Chen, et al. Mathematical model and characteristic analysis of elliptical gears manufactured by circular-arc shaper cutters. *Journal of Mechanical Design*, 2007, 129(2): 210-217.
[7] J G Li, X T Wu, S M Mao. Numerical computing method of noncircular gear tooth profiles generated by shaper cutters. *The International Journal of Advanced Manufacturing Technology*, 2007, 33: 1098-1105.
[8] B T Li, J Hu, D Chen, et al. Numerical algorithm of noncircular gear's tooth profile based on jarvis march. *International Conference on Human Centered Computing*, 2016: 689-694.
[9] L Xia, Y Y Liu, D Z Li, et al. A linkage model and applications of hobbing non-circular helical gears with axial shift of hob. *Mechanism and Machine Theory*, 2013, 70: 32-44.
[10] F Y Zheng, L Hua, X H Han, et al. Linkage model and manufacturing process of shaping noncircular gears. *Mechanism and Machine Theory*, 2016, 96: 192-212.
[11] F LLitvin, P I Gonzalez, K Yukishima, et al. Generation of planar and helical elliptical gears by application of rack-cutter, hob, and shaper. *Computer Methods in Applied Mechanics & Engineering*, 2007, 196 (41-44): 4321-4336.
[12] W M Tan, C B Hu, W J Xian, et al. Concise mathematical model for hobbing noncircular gear and its graphical simulation. *Journal of Mechanical Engineering*, 2001, 37(5): 26-29.
[13] C B Hu, H Y Ding, K M Yan, et al. Simultaneous-control methods of CNC for hobbing non-circular helical gears. *China Mechanical Engineering*, 2004, 15(24): 15-18.
[14] J Han, L L Wu, B Yuan, et al. A novel gear machining CNC design and experimental research. *The International Journal of Advanced Manufacturing Technology*, 2017, 88: 1711-1722.
[15] L L Wu, J Han, Y G Zhu, et al. Noncircular gear continuous generating machining interpolation method and experimental research. *Journal of*

the Brazilian Society of Mechanical Sciences and Engineering, 2017, 39(5): 5171-5180.
[16] S L Wang, S L Sun, J Zhou, et al. Research on mapping rules of hob geometric errors and gear geometric precision. *Journal of Mechanical Engineering*, 2013, 49(19): 119-125.
[17] J Han, D Z Li, X Q Tian, et al. Linkage model and interpolation analysis of helical noncircular gear hobbing. *Journal of the Brazilian Society of Mechanical Sciences and Engineering*, 2020, 42(11): 582.
[18] K D Bouzakis, E Lili, N Michailidis, et al. Manufacturing of cylindrical gears by generating cutting processes: A critical synthesis of analysis methods. *CIRP Annals - Manufacturing Technology*, 2008, 57(2): 676-696.
[19] H J Cao, X G Li, P Chen. *Green high speed dry hobbing process theory and key technology*. Chongqing: Chongqing University Press, 2016.
[20] J Han, D Z Li, L Xia, et al. Analytical study on tooth profile of noncircular gear based on hobbing process simulation. *International Manufacturing Science and Engineering Conference,* Pennsylvania, USA, June 10–14, 2019: V002T03A025.